SCIENCE CHINA
Chemistry

•ARTICLES•

https://doi.org/10.1007/s11426-018-9334-9

A chlorinated low-bandgap small-molecule acceptor for organic solar cells with 14.1% efficiency and low energy loss

Bin Kan[1], Huanran Feng[1], Huifeng Yao[2], Meijia Chang[1], Xiangjian Wan[1], Chenxi Li[1], Jianhui Hou[2*] & Yongsheng Chen[1*]

[1]*State Key Laboratory and Institute of Elemento-Organic Chemistry, The Centre of Nanoscale Science and Technology and Key Laboratory of Functional Polymer Materials, College of Chemistry, Nankai University, Tianjin 300071, China;*
[2]*State Key Laboratory of Polymer Physics and Chemistry, Beijing National Laboratory for Molecular Sciences, CAS Research/Education Center for Excellence in Molecular Sciences, Institute of Chemistry, Chinese Academy of Sciences, Beijing 100190, China*

Received July 12, 2018; accepted July 17, 2018; published online July 26, 2018

A new acceptor-donor-acceptor (A-D-A) type small-molecule acceptor NCBDT-4Cl using chlorinated end groups is reported. This new-designed molecule demonstrates wide and efficient absorption ability in the range of 600–900 nm with a narrow optical bandgap of 1.40 eV. The device based on PBDB-T-SF:NCBDT-4Cl shows a power conversion efficiency (PCE) of 13.1% without any post-treatment, which represents the best result for all as-cast organic solar cells (OSCs) to date. After device optimizations, the PCE was further enhanced to over 14% with a high short-circuit current density (J_{sc}) of 22.35 mA cm^{-2} and a fill-factor (FF) of 74.3%. The improved performance was attributed to the more efficient photo-electron conversion process in the optimal device. To our knowledge, this outstanding efficiency of 14.1% with an energy loss as low as 0.55 eV is among the best results for all single-junction OSCs.

small-molecule acceptor, low-bandgap, chlorinated, high performance

Citation: Kan B, Feng H, Yao H, Chang M, Wan X, Li C, Hou J, Chen Y. A chlorinated low-bandgap small-molecule acceptor for organic solar cells with 14.1% efficiency and low energy loss. *Sci China Chem*, 2018, 61, https://doi.org/10.1007/s11426-018-9334-9

1 Introduction

The state-of-art organic solar cells (OSCs) with bulk heterojunction (BHJ) structures have attracted widespread attention since they are solution-processable, light-weighted and flexible [1–3]. Compared to the widely investigated fullerene derivatives, nonfullerene acceptors (NFAs) have some unique advantages, such as easily-tuned energy levels, wide and efficient light absorption and diverse chemical structures [4–8]. More importantly, it has been demonstrated that NFA based OSCs have great potentials in reducing energy loss due to their weak driving force for exciton separation and enhancing light absorption strength, which are beneficial for obtaining high open-circuit voltage (V_{oc}) and short-circuit current density (J_{sc}) simultaneously [9–13]. Consequently, remarkable achievements have been done in NFAs based OSCs with power conversion efficiencies (PCEs) larger than 14%, surpassing their fullerene-based counterparts [14–18]. These outstanding results are partially owing to the rapid development of novel electron donor and electron acceptor materials in the last few years [19–24].

In particular, low-bandgap small-molecule nonfullerene acceptors (SM-NFAs), which possess the acceptor-donor-acceptor (A-D-A) backbone architecture, play a vital role in the field of NF-OSCs due to their effectively light-harvesting abilities in the visible to near-infrared region (NIR) [25–29]. The A-D-A structured SM-NFAs have the characteristic that their energy levels could be easily tuned by modifying the

*Corresponding authors (email: hjhzlz@iccas.ac.cn; yschen99@nankai.edu.cn)

chemical structures of central unit (D) and/or end groups (A) [30–33]. With these strategies, lots of high-performance low-bandgap SM-NFAs have been reported following the appearance of the fused-ring based ITIC [34–38]. For example, with delicate modifying the chemical structures of D and A units for NFBDT, we reported a low bandgap SM-NFA NCBDT using 4,8-dioctylbenzo[1,2-b:4,5-b′]dithiophene (BDT)-based fused-ring (CBDT) as the core unit (D) and the fluorinated 2-(2,3-dihydro-3-oxo-1H-inden-1-ylidene)propanedinitrile (F-INCN) as the end groups (A) [11,39]. A high PCE above 12% and a J_{sc} over 20 mA cm^{-2} were achieved for the PBDB-T:NCBDT based device, suggesting the superiority of CBDT unit for designing novel low-bandgap acceptors. As reported, modifications of A units provide another platform for fine-tuning NFAs with enhanced OSC performance [17,18]. Since the chlorine atom with high electron affinity, larger dipole moment and effective delocalization of π electrons, the introduction of chlorine atom to the INCN unit may be a wise choice to construct high-performance small-molecule acceptors (SMAs).

In this study, we developed and synthesized NCBDT-4Cl, a new A-D-A type small-molecule acceptor NCBDT-4Cl based on the large planar central unit CBDT and the chlorinated INCN end groups. Figure 1(a) depicts the specific chemical structure of NCBDT-4Cl. It shows strong absorption ability in the range of 600–900 nm and a low optical bandgap (E_g^{opt}) of 1.40 eV. A fluorinated wide-bandgap polymer PBDB-T-SF (Figure 1(a)) with relatively deep highest occupied molecular orbital (HOMO) energy level was selected as electron donor from the perspective of energy levels and absorption matching [40]. As results, the as-cast device based on PBDB-T-SF:NCBDT-4Cl exhibits an encouraging efficiency of 13.1% and a low energy loss of 0.52 eV, which represents the best performance for all as-cast OSCs. Furthermore, an outstanding PCE over 14% with a V_{oc} of 0.85 V, a high J_{sc} of 22.35 mA cm^{-2} and a fill-factor (FF) of 74.3% were achieved after device optimizations. The above result is one of the very few reported OSCs with efficiency over 14%.

2 Experimental

2.1 Materials

All reactions and manipulations were carried out under argon atmosphere with the use of standard Schlenk techniques. (4,8-Dioctylbenzo[1,2-b:4,5-b']dithiophene-2,6-diyl)bis(trimethylstannane) was purchased from Solarmer Material Inc. (Beijing, China). 2-(5,6-Dichloro-3-oxo-2,3-dihydro-1H-inden-1-ylidene)malononitrile was purchased from Derthon optoelectronic materials science technology Co LTD (Shenzhen, China). All starting materials were purchased from commercial suppliers and used without further purification unless indicated otherwise.

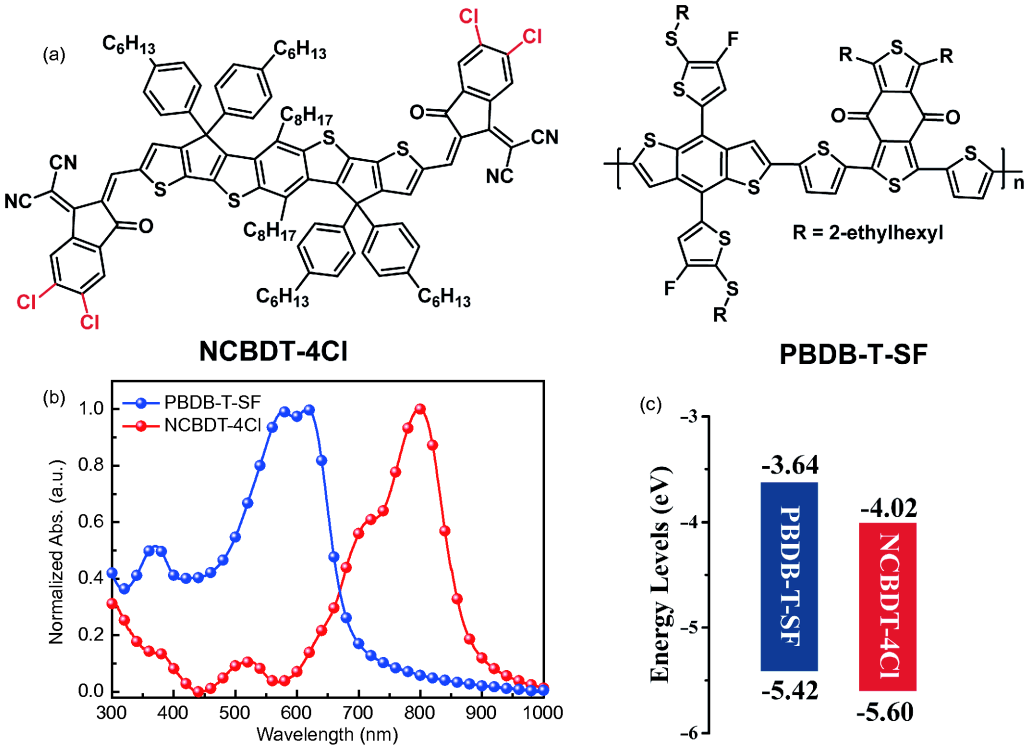

Figure 1 (a) Chemical structures of PBDB-T-SF and NCBDT-4Cl; (b) normalized absorption spectra of PBDB-T-SF and NCBDT-4Cl neat films; (c) the energy diagrams of PBDB-T-SF and NCBDT-4Cl in the thin-film state calculated from CV results (color online).

2.2 Synthesis of NCBDT-4Cl

Under the protection of argon, the dialdehyde compound DFCBDT (130 mg, 0.10 mmol) and 2-(5,6-dichloro-3-oxo-2,3-dihydro-1H-inden-1-ylidene)malononitrile (104 mg, 0.40 mmol) was dissolved in a dry $CHCl_3$ (40 mL) solution. After adding 0.5 mL pyridine, the mixture was stirring at room temperature for overnight and then poured into water. The mixture was extracted with $CHCl_3$ for twice (30 mL×2), and the combined organic layer was dried with anhydrous Na_2SO_4 for 1 h. After removal of solvent, the crude product was purified by silica gel using petroleum ether/$CHCl_3$ (1:2) as eluent to give NCBDT-4Cl as a dark-blue solid (148 mg, 82%). ^{1}H NMR (400 MHz, $CDCl_3$): δ 8.79 (s, 2H), 8.73 (s, 2H), 7.88 (s, 2H), 7.59 (s, 2H), 7.31 (d, 8H), 7.12 (d, 8H), 2.80 (t, 4H), 2.58 (t, 8H), 1.64–1.53 (m, 8H), 1.35–1.22 (m, 40H), 1.07–1.00 (m, 4H), 0.98–0.72 (m, 18H), 0.72 (br, 4H). ^{13}C NMR (100 MHz, $CDCl_3$): δ 186.15, 165.35, 158.26, 158.11, 155.42, 145.84, 142.52, 140.90, 140.45, 139.53, 139.23, 138.83, 138.74, 138.60, 135.97, 134.70, 132.57, 132.41, 128.71, 128.55, 126.92, 125.05, 120.40, 68.84, 63.81, 35.53, 34.81, 32.03, 31.70, 31.15, 30.66, 29.51, 28.91, 22.76, 22.59, 14.19. HR-MS: calcd for $C_{110}H_{110}Cl_4N_4O_2S_4$ $[M+H]^+$, 1790.1480; found: 1789.6202.

2.3 Instruments and characterization

The ^{1}H and ^{13}C NMR spectra were recorded on a Bruker AV400 Spectrometer (Germany). The thermogravimetric analysis (TGA) was carried out on a NETZSCH STA 409PC instrument (Germany) under purified nitrogen gas flow with the heating rate of 10 °C min^{-1}. UV-Vis spectra were obtained with a JASCO V-570 spectrophotometer (Japan). The geometry structures of NCBDT-4Cl were optimized by using density functional theory calculations (B3LYP/6-31G*), and the frequency analysis was followed to assure that the optimized structures were stable states. All calculations were carried out using Gaussian 09.

Cyclic voltammetry (CV) experiments were performed with a LK98B II Microcomputer-based Electrochemical Analyzer (China). All CV measurements were carried out at room temperature with a conventional three-electrode configuration employing a glassy carbon electrode as the working electrode, a saturated calomel electrode (SCE) as the reference electrode, and a Pt wire as the counter electrode. Dichloromethane was distilled from calcium hydride under dry nitrogen immediately prior to use. tetrabutylammonium phosphorus hexafluoride (Bu_4NPF_6, 0.1 M) in dry CH_3CN was used as the supporting electrolyte, and the scan rate was 50 mV s^{-1}. The HOMO and lowest unoccupied molecular orbital (LUMO) energy levels were calculated from the onset oxidation potential and the onset reduction potential, using the equation E_{HOMO}=−(4.80+E^{ox}_{onset}), E_{LUMO}= −(4.80+E^{re}_{onset}).

Atomic force microscopy (AFM) was performed using Multimode 8 atomic force microscope in tapping mode (Germany). The transmission electron microscopy (TEM) investigation was performed on Philips Technical G^2 F20 at 200 kV (America & Netherlands). The specimen for TEM measurement was prepared by spin casting the blend solution on ITO/PEDOT:PSS substrate, then floating the film on a water surface, and transferring to TEM grids. Two-dimensional grazing-incidence wide-angle X-ray scattering (2D-GIXD) was performed at beamline BL14B1 at Shanghai Synchrotron Radiation Facility (SSRF).

Space charge limited current (SCLC) mobility was measured using a diode configuration and fitting the results to a space charge limited form, where SCLC equation is described by:

$$J = \frac{9\varepsilon_0\varepsilon_r\mu_0 V^2}{8L^3}$$

where J is the current density, L is the film thickness of the active layer, μ_0 is the mobility, ε_r is the relative dielectric constant of the transport medium, ε_0 is the permittivity of free space (8.85×10^{-12} F m^{-1}), V (V=V_{appl}−V_{bi}) is the internal voltage in the device, where V_{appl} is the applied voltage to the device and V_{bi} is the built-in voltage due to the relative work function difference of the two electrodes.

2.4 Solar cell fabrication and testing

The devices were fabricated with a structure of glass/ITO/PEDOT:PSS/PBDB-T-SF:NCBDT-4Cl/PDINO/Al. The ITO-coated glass substrates were cleaned by ultrasonic treatment in detergent, deionized water, acetone, and isopropyl alcohol under ultra-sonication for 15 min each and subsequently dried by a nitrogen blow. A thin layer of PEDOT:PSS (Clevios P VP AI 4083, filtered at 0.45 μm) was spin-coated at 3000 r min^{-1} onto ITO surface. After baked at 150 °C for 20 min, the substrates were transferred into an argon-filled glove box. Subsequently, the active layer was spin-coated from donor and acceptor in chloroform (0.2% 1,8-diiodooctane (DIO)) solution on the ITO/PEDOT:PSS substrate. The active layer was further treated with thermal annealing at 110 °C for 10 min. PDINO (1 mg mL^{-1} in CH_3OH) was spin-coated at 3000 r min^{-1} for 40 s on the active layer. Finally, a 60 nm Al layer was deposited under high vacuum (<1.5×10^{-4} Pa). The effective area of each cell was 4 mm^2. The current density-voltage (*J-V*) curves of photovoltaic devices were obtained by a Keithley 2400 source-measure unit (USA). The photocurrent was measured under illumination simulated 100 mW cm^{-2} AM 1.5G irradiation using an Oriel 96000 solar simulator, calibrated with a standard Si solar cell (Japan). External quantum efficiencies were measured using Stanford Research Systems SR810 lock-in amplifier.

3 Results and discussion

3.1 Synthesis and thermal properties

The synthetic route of NCBDT-4Cl is presented as Scheme 1, and the detail synthetic procedures are provided in the experimental section. The dialdehyde compound DFCBDT is prepared based on our previous work [11]. NCBDT-4Cl was obtained as a dark-blue solid by the Knoevenagel condensation reaction between DFCBDT and Cl-INCN, and its chemical structure was fully characterized by NMR and HR-MS. The molecular structure of NCBDT-4Cl was optimized using density functional theory at the B3LYP/6-31G* level, and its optimized geometry is displayed as Figure S1 (Supporting Information online). NCBDT-4Cl shows highly coplanar conjugation backbone structure, which should be beneficial for the π-π stacking and charge transport. Due to the existence of the bulky side chains, NCBDT-4Cl displays excellent solubility in common organic solvents (e.g, chloroform and chlorobenzene), despite the addition of four chlorine atoms. The thermogravimetric analysis (TGA) was used to evaluate the thermal stability of NCBDT-4Cl under nitrogen atmosphere. Figure S2 shows that NCBDT-4Cl did not decompose over 300 °C, suggesting its good thermal stability in the application of OSCs.

3.2 Photo-physical and electrochemical properties

As seen in Figure S3, NCBDT-4Cl in diluted $CHCl_3$ solution shows a maximum absorption peak at 749 nm and a high absorption coefficient of 2.1×10^5 M^{-1} cm^{-1}. The normalized thin-film absorption spectra of NCBDT-4Cl and polymer donor PBDB-T-SF are depicted in Figure 1(b). Compared to its solution spectrum, NCBDT-4Cl in solid state exhibits approximately red-shifted 50 nm with an absorption peak at 798 nm and broaden absorption range from 600 to 900 nm. The absorption spectrum of polymer donor PBDB-T-SF is mainly in the range of 400–700 nm, thus the combination of PBDB-T-SF and NCBDT-4Cl offers a quite well complementary absorption extended to the NIR range, which is a prerequisite for obtaining high J_{sc}. The absorption onset of NCBDT-4Cl film is 885 nm, corresponding to a low E_g^{opt} of 1.40 eV, which calculated from the equation of E_g^{opt}=1240/λ_{onset}.

The energy levels of NCBDT-4Cl and PBDB-T-SF thin films were tested by cyclic voltammetry (CV) under the identical condition, and their CV curves were shown as Figure S4. The HOMO and LUMO energy levels of NCBDT-4Cl are calculated to be −5.60 and −4.02 eV, respectively. As shown in Figure 1(c), the HOMO energy offset (ΔHOMO) between the donor and acceptor is 0.18 eV, which is below the empirical value of 0.30 eV but large enough for the charge generation from the acceptor to the donor in the nonfullerene based devices [19,41]. More importantly, the small ΔHOMO is considered to be beneficial in reducing the energy loss, which is of great importance for obtaining high V_{oc} of the devices [7,33].

3.3 OSC performance

Solution-processed devices were constructed using NCBDT-4Cl as electron acceptor with the conventional configuration of indium tin oxides (ITO)/poly(3,4-ethylenedioxythiopene): poly(styrenesulfonate) (PEDOT:PSS)/PBDB-T-SF:NCBDT-4Cl/perylene diimide functionalized with amino *N*-oxide (PDINO)/Al, where PDINO was selected as electron transport layer (Table S1, Supporting Information online) [42]. The weight ratio of donor and acceptor was controlled to be 1:1 according to the previous work [40], and the thickness of the active layer was optimized to be ~110 nm by tuning the rotation speed of spin-coating. Surprisingly, the as-cast device delivers a V_{oc} of 0.885 V, a J_{sc} of 20.81 mA cm^{-2} and a FF of 70.9%, resulting in an outstanding PCE of 13.1%, which represents the highest result for all as-cast devices. To further improve the performance, 1,8-diiodooctane (DIO, 0.2%, *v*/*v*) was used as solvent additive to tune the morphology. The active layer was then followed by thermal annealing at 110 °C for 10 min to obtain the best performance (Table S2). Consequently, a PCE of 14.1% with an enhanced J_{sc} of 22.35 mA cm^{-2} and a high FF near 75% were achieved for the PBDB-T-SF:NCBDT-4Cl based device. Though the V_{oc} of the device is slightly decreased to 0.85 V, the energy loss (E_{loss}=E_g^{opt}–eV_{oc}) is still only 0.55 eV. To our knowledge, this remarkable PCE over 14% with E_{loss} around 0.55 eV is among the best of single-junction OSCs. The

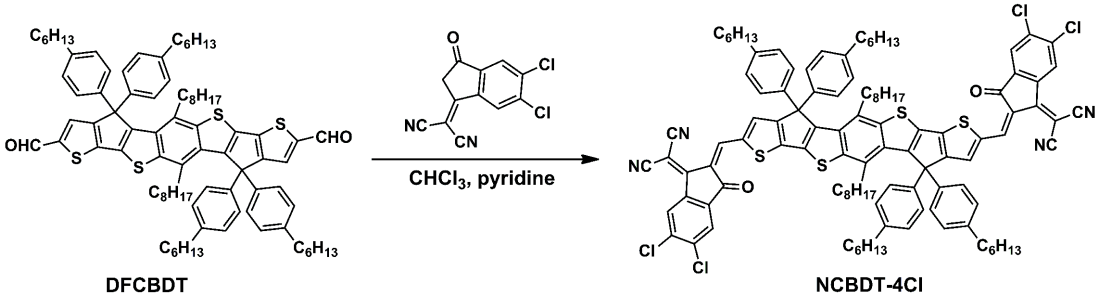

Scheme 1 Synthetic route of NCBDT-4Cl.

current density-voltage (*J*-V) curves and the performance histogram of the counts of the as-cast and optimal devices are displayed in Figure 2(a) and (b), respectively. Table 1 summarizes their corresponding device parameters.

The external quantum efficiency (EQE) curves of the as-cast and optimal devices were studied to verify their high J_{sc} values. As observed in Figure 2(c), both devices yield broad photo-current responses and high EQE values which covered a wide range. The calculated J_{sc} of the as-cast and optimal devices, integrated from their corresponding EQE curves, are 20.48 and 21.63 mA cm^{-2}, respectively. These J_{sc} values are within accountable mismatch with those obtained from their *J-V* curves. Compared to the as-cast device, the optimal device shows higher EQE values in the range of 450–880 nm. In addition, large EQE values exceeding 75% across the range 550–650 nm with a maximum value up to 79% were achieved for the optimal device. Importantly, EQE with reasonably high values could be achieved in the range of 700–850 nm which attribute to the contribution of NCBDT-4Cl, indicating the hole transfer process from the acceptor to polymer donor is highly efficient despite of the small ΔHOMO between them. In order to compare the exciton disassociation and charge collection properties in the as-cast and optimal devices, their photocurrent (J_{ph}) versus the effective applied voltage (V_{eff}) were investigated using the reported method shown as Figure 2(d) [43]. The charge dissociation probability ($P(E,T)$) could be estimated from the ratio of J_{ph}/J_{sat}. Under the short-circuit and maximal power output conditions, the optimal device gives higher $P(E,T)$ values (97% and 87%) than those of the as-cast device (92% and 81%). All above suggest that more efficient photoelectron conversion process is occurred in the optimal device, leading to higher J_{sc} and FF.

3.4 Morphologies characterization

The morphological evolutions for the as-cast and optimal blend films were studied by AFM and TEM. Their AFM images (Figure 3(a, b)) show that both blend films are uniform and smooth with low root-mean-square surface roughness (R_q) values of 1.24 and 1.41 nm, respectively. No large phase separation or over-aggregation could be ob-

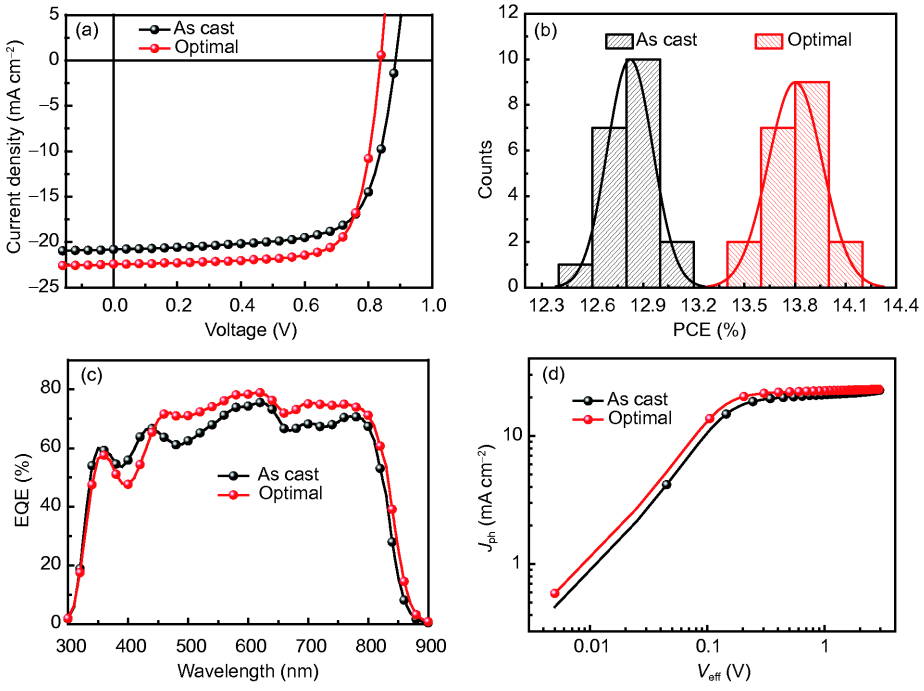

Figure 2 (a) Current density-voltage (*J*-V) curves of the as-cast and optimal devices based on PBDB-T-SF:NCBDT-4Cl; (b) the performance histogram of the counts of the as-cast and optimal devices; (c) the EQE curves of the as-cast and optimal devices; (d) J_{ph} versus V_{eff} of the as-cast and optimal devices, respectively (color online).

Table 1 OSC parameters of the as-cast and optimal devices using the conventional device configuration under the illumination of AM 1.5G (100 mW cm^{-2}), and the average data were obtained from 20 devices

Conditions	V_{oc} (V)	J_{sc} (mA cm^{-2})	FF (%)	PCE (%)	E_{loss} (eV)
As-cast	0.885 (0.880±0.003)	20.81 (20.38±0.24)	70.9 (70.2±0.4)	13.1 (12.8±0.1)	0.52
Optimal [a)]	0.851 (0.848±0.003)	22.35 (22.05±0.18)	74.3 (74.0±0.2)	14.1 (13.8±0.2)	0.55

a) 0.2% DIO + thermal annealing at 110 °C for 10 min.

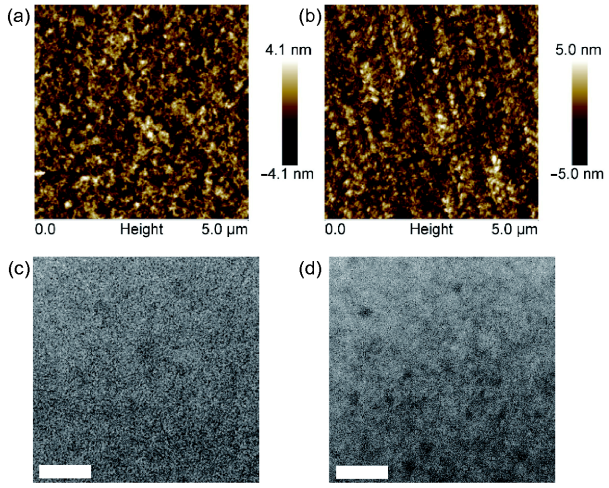

Figure 3 AFM and TEM images for (a, c) as-cast blend film and (b, d) optimal blend film. The scale bar is 200 nm (color online).

served. Compared to the AFM and TEM images of the as-cast film, the images of the optimal film display more continual and distinctive grain-like domains, which is supposed to be beneficial for charge transport and collection. Afterwards, their charge transport properties were measured by space-charge-limited current (SCLC) method, and the electron-only and hole-only device structures are ITO/ZnO/active layer/Al and ITO/PEDOT:PSS/active layer/Au, respectively. The electron and hole mobilities for the as-cast film are calculated to be 1.13×10^{-4} and 1.83×10^{-4} cm^{-2} V^{-1} s^{-1}, respectively. While, the optimal film exhibits higher and more balanced electron and hole mobilities (1.85×10^{-4} and 2.25×10^{-4} cm^{-2} V^{-1} s^{-1}, respectively), leading its better J_{sc} and FF.

Two-dimensional grazing-incidence wide-angle X-ray scattering (2D-GIXD) method was performed to investigate the molecular packing behaviors of the neat and blend films. Figure 4(a, b) displays the diffraction patterns of NCBDT-4Cl and PBDB-T-SF neat films, and Figure S4 presents their line-cut profiles. NCBDT-4Cl film shows an alkyl-to-alkyl diffraction peak (100) along the q_{xy} direction and an obvious π-π stacking diffraction peak (010) along the q_z direction, indicative of its preferred face-on molecular orientation [44]. For NCBDT-4Cl acceptor, its (100) and (010) peaks are located at 0.28 and 1.80 $Å^{-1}$, corresponding an alkyl-to-alkyl distance of 22.4 Å and π-π stacking distance of 3.49 Å, respectively. Polymer donor PBDB-T-SF prefers the same face-on orientation, which could be derived from its clear (010) peak along the q_z direction. As seen in Figure 4(c, d), the as-cast and optimal blend films both display broad and combined (010) diffraction peak along the q_z direction, which implies that NCBDT-4Cl and PBDB-T-SF still adopt the face-on orientation in the blend films. Compared to the as-cast film, the optimal film not only shows combined (100) diffraction peak located at q_{xy}=0.29 $Å^{-1}$ but also higher order diffraction peak along the q_{xy} direction, indicating enhanced molecular packing. All these contribute to better charge transport abilities of the optimal film, which is in accordance with its higher charge mobilities.

4 Conclusions

In summary, a new A-D-A nonfullerene acceptor NCBDT-

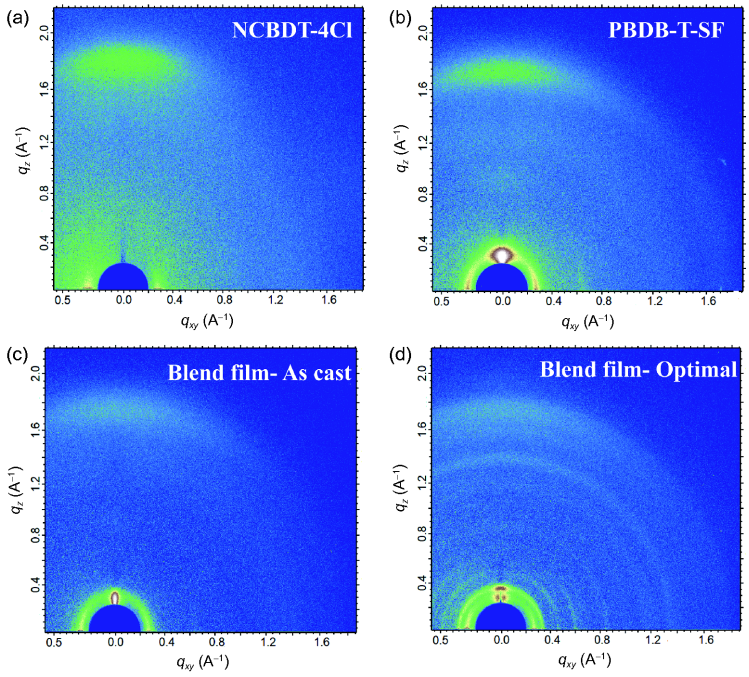

Figure 4 2D-GIXD patterns for (a, b) NCBDT-4Cl and PBDB-T-SF neat films, and (c, d) PBDB-T-SF:NCBDT-4Cl blend films, respectively (color online).

4Cl with chlorinated end groups was synthesized and fully characterized. NCBDT-4Cl demonstrates a low optical bandgap of 1.40 eV and effective absorption ranging from 600 to 900 nm. By blending with a wide bandgap polymer donor PBDB-T-SF, the device without any post-treatment gives an efficiency of 13.1%, the best result for all as-cast OSCs to date. It should be pointed out that the extraordinary performance of the as-cast device is significant to the future applications of OSCs. Furthermore, a remarkable PCE of 14.1% with a V_{oc} of 0.85 V, a high J_{sc} of 22.35 mA cm^{-2} and a FF of 74.3% were achieved after solvent additive along with thermal annealing treatment. The improved performance can be ascribed to the optimized active layer morphology and better charge transport process. To the best of our knowledge, this high efficiency over 14% with such a low energy loss of 0.55 eV is one of the best results for all single-junction OSCs. Considering the versatility of donor and SM-NFA materials, higher PCE will be realized by further reducing the energy loss and broadening the absorption range.

Acknowledgements This work was supported by the National Natural Science Foundation of China (91633301, 51773095), MoST of China (2014CB643502), Tianjin city (17JCJQJC44500, 17CZDJC31100) and 111 Project (B12015). The authors also thank beamline BL14B1 (Shanghai Synchrotron Radiation Facility) for providing the beam time.

Conflict of interest The authors declare that they have no conflict of interest.

Supporting information The supporting information is available online at http://chem.scichina.com and http://link.springer.com/journal/11426. The supporting materials are published as submitted, without typesetting or editing. The responsibility for scientific accuracy and content remains entirely with the authors.

1 Yu G, Gao J, Hummelen JC, Wudl F, Heeger AJ. *Science*, 1995, 270: 1789–1791
2 Li G, Zhu R, Yang Y. *Nat Photon*, 2012, 6: 153–161
3 Dou L, Liu Y, Hong Z, Li G, Yang Y. *Chem Rev*, 2015, 115: 12633–12665
4 McAfee SM, Topple JM, Hill IG, Welch GC. *J Mater Chem A*, 2015, 3: 16393–16408
5 Nielsen CB, Holliday S, Chen HY, Cryer SJ, McCulloch I. *Acc Chem Res*, 2015, 48: 2803–2812
6 Li S, Liu W, Li CZ, Shi M, Chen H. *Small*, 2017, 13: 1701120
7 Hou J, Inganäs O, Friend RH, Gao F. *Nat Mater*, 2018, 17: 119–128
8 Yang Y, Zhang ZG, Bin H, Chen S, Gao L, Xue L, Yang C, Li Y. *J Am Chem Soc*, 2016, 138: 15011–15018
9 Liu J, Chen S, Qian D, Gautam B, Yang G, Zhao J, Bergqvist J, Zhang F, Ma W, Ade H, Inganäs O, Gundogdu K, Gao F, Yan H. *Nat Energy*, 2016, 1: 16089
10 Cheng P, Zhang M, Lau TK, Wu Y, Jia B, Wang J, Yan C, Qin M, Lu X, Zhan X. *Adv Mater*, 2017, 29: 1605216
11 Kan B, Zhang J, Liu F, Wan X, Li C, Ke X, Wang Y, Feng H, Zhang Y, Long G, Friend RH, Bakulin AA, Chen Y. *Adv Mater*, 2018, 30: 1704904
12 Fei Z, Eisner FD, Jiao X, Azzouzi M, Röhr JA, Han Y, Shahid M, Chesman ASR, Easton CD, McNeill CR, Anthopoulos TD, Nelson J, Heeney M. *Adv Mater*, 2018, 30: 1705209
13 Yao H, Qian D, Zhang H, Qin Y, Xu B, Cui Y, Yu R, Gao F, Hou J. *Chin J Chem*, 2018, 36: 491–494
14 Xiao Z, Jia X, Ding L. *Sci Bull*, 2017, 62: 1562–1564
15 Zhang S, Qin Y, Zhu J, Hou J. *Adv Mater*, 2018, 30: 1800868
16 Cui Y, Yao HF, Yang CY, Zhang SQ, Hou JH. *Acta Polym Sin*, 2018, 2: 223–230
17 Zhang Y, Yao H, Zhang S, Qin Y, Zhang J, Yang L, Li W, Wei Z, Gao F, Hou J. *Sci China Chem*, 2018, 61: doi: 10.1007/s11426-018-9260-2
18 Zhang H, Yao H, Hou J, Zhu J, Zhang J, Li W, Yu R, Gao B, Zhang S, Hou J. *Adv Mater*, 2018, 29: 1800613
19 Bin H, Gao L, Zhang ZG, Yang Y, Zhang Y, Zhang C, Chen S, Xue L, Yang C, Xiao M, Li Y. *Nat Commun*, 2016, 7: 13651
20 Bin H, Zhong L, Zhang ZG, Gao L, Yang Y, Xue L, Zhang J, Zhang Z, Li Y. *Sci China Chem*, 2016, 59: 1317–1322
21 Zhang H, Liu Y, Sun Y, Li M, Ni W, Zhang Q, Wan X, Chen Y. *Sci China Chem*, 2017, 60: 366–369
22 Baran D, Ashraf RS, Hanifi DA, Abdelsamie M, Gasparini N, Röhr JA, Holliday S, Wadsworth A, Lockett S, Neophytou M, Emmott CJM, Nelson J, Brabec CJ, Amassian A, Salleo A, Kirchartz T, Durrant JR, McCulloch I. *Nat Mater*, 2017, 16: 363–369
23 Xu SJ, Zhou Z, Liu W, Zhang Z, Liu F, Yan H, Zhu X. *Adv Mater*, 2017, 29: 1704510
24 Fan Q, Su W, Wang Y, Guo B, Jiang Y, Guo X, Liu F, Russell TP, Zhang M, Li Y. *Sci China Chem*, 2018, 61: 531–537
25 Liu F, Zhou Z, Zhang C, Vergote T, Fan H, Liu F, Zhu X. *J Am Chem Soc*, 2016, 138: 15523–15526
26 Yao H, Chen Y, Qin Y, Yu R, Cui Y, Yang B, Li S, Zhang K, Hou J. *Adv Mater*, 2016, 28: 8283–8287
27 Dai S, Zhao F, Zhang Q, Lau TK, Li T, Liu K, Ling Q, Wang C, Lu X, You W, Zhan X. *J Am Chem Soc*, 2017, 139: 1336–1343
28 Shi X, Zuo L, Jo SB, Gao K, Lin F, Liu F, Jen AKY. *Chem Mater*, 2017, 29: 8369–8376
29 Yao H, Cui Y, Yu R, Gao B, Zhang H, Hou J. *Angew Chem Int Ed*, 2017, 56: 3045–3049
30 Cheng P, Li G, Zhan X, Yang Y. *Nat Photon*, 2018, 12: 131–142
31 Yang F, Li C, Lai W, Zhang A, Huang H, Li W. *Mater Chem Front*, 2017, 1: 1389–1395
32 Qiu N, Zhang H, Wan X, Li C, Ke X, Feng H, Kan B, Zhang H, Zhang Q, Lu Y, Chen Y. *Adv Mater*, 2017, 29: 1604964
33 Zhang G, Zhao J, Chow PCY, Jiang K, Zhang J, Zhu Z, Zhang J, Huang F, Yan H. *Chem Rev*, 2018, 118: 3447–3507
34 Lin Y, Wang J, Zhang ZG, Bai H, Li Y, Zhu D, Zhan X. *Adv Mater*, 2015, 27: 1170–1174
35 Li S, Ye L, Zhao W, Zhang S, Mukherjee S, Ade H, Hou J. *Adv Mater*, 2016, 28: 9423–9429
36 Li S, Ye L, Zhao W, Liu X, Zhu J, Ade H, Hou J. *Adv Mater*, 2017, 29: 1704051
37 Yi YQQ, Feng H, Chang M, Zhang H, Wan X, Li C, Chen Y. *J Mater Chem A*, 2017, 5: 17204–17210
38 Yan C, Barlow S, Wang Z, Yan H, Jen AKY, Marder SR, Zhan X. *Nat Rev Mater*, 2018, 3: 18003
39 Kan B, Feng H, Wan X, Liu F, Ke X, Wang Y, Wang Y, Zhang H, Li C, Hou J, Chen Y. *J Am Chem Soc*, 2017, 139: 4929–4934
40 Zhao W, Li S, Yao H, Zhang S, Zhang Y, Yang B, Hou J. *J Am Chem Soc*, 2017, 139: 7148–7151
41 Zheng Z, Awartani OM, Gautam B, Liu D, Qin Y, Li W, Bataller A, Gundogdu K, Ade H, Hou J. *Adv Mater*, 2017, 29: 1604241
42 Zhang ZG, Qi B, Jin Z, Chi D, Qi Z, Li Y, Wang J. *Energy Environ Sci*, 2014, 7: 1966–1973
43 Blom P, Mihailetchi V, Koster L, Markov D. *Adv Mater*, 2007, 19: 1551–1566
44 Müller-Buschbaum P. *Adv Mater*, 2014, 26: 7692–7709